11-12-2004

Structural Mimicry in Class A G Protein-coupled Receptor Rotamer Toggle Switches

Sean D. McAllister
California Pacific Medical Center Research Institute

Dow P. Hurst
Kennesaw State University

Judy Barnett-Norris
Kennesaw State University

Diane L. Lynch
Kennesaw State University

Patricia H. Reggio
Kennesaw State University

See next page for additional authors

Recommended Citation

McAllister SD, Hurst DP, Barnett-Norris J, Lynch D, Reggio PH, Abood ME. 2004. Structural mimicry in class A G protein-coupled receptor rotamer toggle switches. Journal of Biological Chemistry 279(46):48024-37.

THE JOURNAL OF BIOLOGICAL CHEMISTRY
Vol. 279, No. 46, Issue of November 12, pp. 48024–48037, 2004
Printed in U.S.A.

Structural Mimicry in Class A G Protein-coupled Receptor Rotamer Toggle Switches

THE IMPORTANCE OF THE F3.36(201)/W6.48(357) INTERACTION IN CANNABINOID CB_1 RECEPTOR ACTIVATION*

Received for publication, June 15, 2004, and in revised form, August 19, 2004
Published, JBC Papers in Press, August 23, 2004, DOI 10.1074/jbc.M406648200

Sean D. McAllister‡, Dow P. Hurst§‖, Judy Barnett-Norris§‖, Diane Lynch§‖, Patricia H. Reggio§‖, and Mary E. Abood‡¶

From the ‡California Pacific Medical Center Research Institute, San Francisco, California 94115 and §Kennesaw State University, Kennesaw, Georgia 30144

In this study, we tested the hypothesis that a CB_1 TMH3-4-5-6 aromatic microdomain, which includes F3.25(190), F3.36(201), W5.43(280), and W6.48(357), is centrally involved in CB_1 receptor activation, with the F3.36(201)/W6.48(357) interaction key to the maintenance of the CB_1-inactive state. We have shown previously that when F3.36(201), W5.43(280), and W6.48(357) are individually mutated to alanine, a significant reduction in ligand binding affinity is observed in the presence of WIN 55,212-2 and SR141716A but not CP55,940 and anandamide. In the work presented here, we report a detailed functional analysis of the F3.36(201)A, F3.25(190)A, W5.43(280)A, and W6.48(357)A mutant receptors in stable cell lines created in HEK cells for agonist-stimulated guanosine 5′-3-*O*-(thio)triphosphate (GTPγS) binding and GIRK1/4 channel current effects in *Xenopus* oocytes where the mutant proteins were expressed transiently. The F3.36(201)A mutation showed statistically significant increases in ligand-independent stimulation of GTPγS binding *versus* wild type CB_1, although basal levels for the W6.48(357)A mutant were not statistically different from wild type CB_1. F3.36(201)A demonstrated a limited activation profile in the presence of multiple agonists. In contrast, enhanced agonist activation was produced by W6.48(357)A. These results suggest that a F3.36(201)/W6.48(357)-specific contact is an important constraint for the CB_1-inactive state that may need to break during activation. Modeling studies suggest that the F3.36(201)/W6.48(357) contact can exist in the inactive state of CB_1 and be broken in the activated state via a χ_1 rotamer switch (F3.36(201) trans, W6.48(357) g+) → (F3.36(201) g+, W6.48(357) trans). The F3.36(201)/W6.48(357) interaction therefore may represent a "toggle switch" for activation of CB_1.

The cannabinoid CB_1 receptor belongs to the class A rhodopsin-like family of G protein-coupled receptors (GPCRs)[1] (see helix net, Fig. 1) (2). The availability of high resolution crystal structures of rhodopsin (Rho) (3, 4) (Protein Data Bank accession code 1GZM) and the availability of biophysical data on the conformational changes that occur when rhodopsin and other class A receptors are activated (6–8) have greatly aided the study of structure-function relationships in class A GPCRs. Ballesteros *et al.* (9) have proposed that "structural mimicry" may occur in GPCRs such that different amino acids or alternate microdomains in class A receptors (*e.g.* the amine receptors) can support similar deviations from the regular α-helical structure seen in Rho, thereby resulting in similar tertiary structures. In the work presented here, we provide evidence that "structural (functional) mimicry" by alternate microdomains may also support the core function of signaling activation through transmembrane helix conformational change in the class A family.

There is a growing body of evidence in the literature that activation of GPCRs is accompanied by rigid domain motions and rotations of transmembrane helices (TMHs) 3 and 6 (6–8). At their intracellular ends, TMHs 3 and 6 in Rho are constrained by an E3.49(134)/R3.50(135)/E6.30 (247) salt bridge that limits the relative mobility of the cytoplasmic ends of TMH3 and TMH6 in the inactive state (3) and acts like an "ionic lock" (10, 11). During activation, P6.50 of the highly conserved CW*X*P motif in TMH6 of GPCRs may act as a flexible hinge, permitting TMH6 to straighten upon activation, moving its intracellular end away from TMH3 and upwards toward the lipid bilayer (12).

Khorana and co-workers (13) have reported that even in the dark (inactive) state of Rho, only some strong constraints exist, whereas the majority of the molecule experiences conformational flexibility. Therefore, light activation of Rho does not require the breaking and forming of thousands of specific contacts within nanoseconds, rather only a few specific contacts restricting the inactive state, including indole side chain contacts of tryptophan residues, need to break on activation. These changes can then be transmitted through the entire membrane protein because of its dynamic plasticity. One of the tryptophan residues that Khorana and co-workers (13) have reported to be restricted is W6.48(265). In the dark (inactive) state of Rho, the β-ionone ring of 11-*cis*-retinal is close to W6.48(265) of the

* This work has been supported by National Institutes on Drug Abuse Grants DA09978, DA05274 (to M. E. A.), DA00489, and DA03934 (to P. H. R.). The costs of publication of this article were defrayed in part by the payment of page charges. This article must therefore be hereby marked "*advertisement*" in accordance with 18 U.S.C. Section 1734 solely to indicate this fact.

‖ Current address: University of North Carolina, Greensboro, NC 27402.

¶ To whom correspondence should be addressed: Forbes Norris ALS/MDA Research Center, 2351 Clay St, Suite 416, California Pacific Medical Center Research Institute, San Francisco, CA 94115. Tel.: 415-600-3607; Fax: 415-563-7325; E-mail: mabood@cooper.cpmc.org.

[1] The abbreviations used are: GPCR, G protein-coupled receptor; CB, cannabinoid; TMH, transmembrane helix; GIRK, G protein-coupled inwardly rectifying potassium; Rho, rhodopsin; WT, wild type; GTPγS, guanosine 5′-3-*O*-(thio)triphosphate; CM, conformational memories.

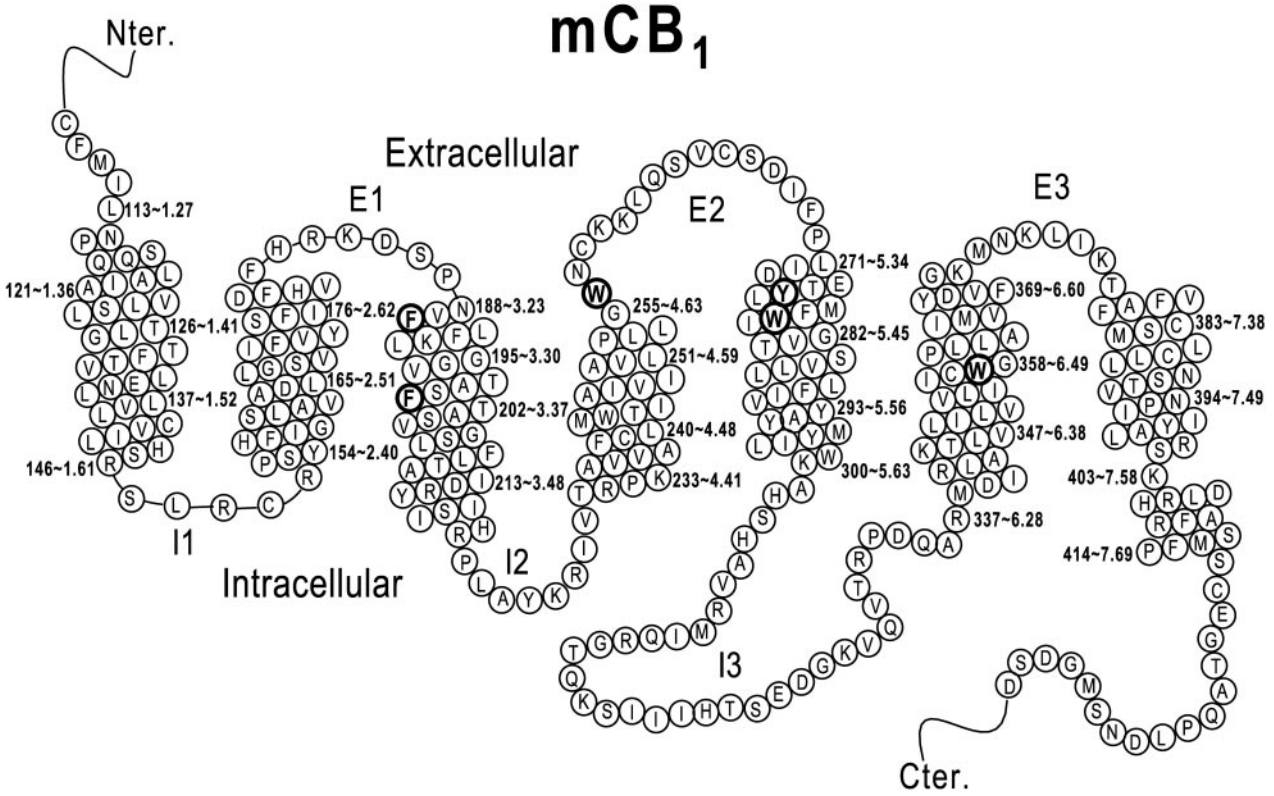

FIG. 1. **A helix net representation of the sequence of the mouse CB_1 receptor.** The amino acids of the TMH3-4-5-6 aromatic microdomain are highlighted in *boldface*.

CW*X*P motif on TMH F and helps constrain it in a χ_1 = g+ conformation (3). In the light-activated state, the β-ionone ring moves away from TMH F and toward TMH D where it resides close to A4.58(169) (14). This movement releases the constraint on W6.48(265), making it possible for W6.48(265) to undergo a conformational change. Lin and Sakmar (15) reported that perturbations in the environment of W6.48(265) of Rho occur during the conformational change concomitant with receptor activation. This suggests that the conformation of W6.48(265) when Rho is in its inactive/ground state (R; χ_1 = g+) changes during activation (*i.e.* W6.48(265) χ_1 g+ $\rightarrow$ trans) (16).

In the class A cationic neurotransmitter receptors, a highly conserved cluster of aromatic amino acids is found on TMH6 that faces the binding site crevice bracketing W6.48 (F6.44, W6.48, F6.51, and F6.52) (16). Shi *et al*. (16) have proposed that an aromatic at 6.52 (F6.52) in the β_2-adrenergic receptor may serve to constrain W6.48 in its inactive state (*i.e.* g+ χ_1) and is part of a rotamer toggle switch (C6.47 trans/W6.48 g+/F6.52 g+ $\rightarrow$ C6.47 g+/W6.48 trans/F6.52 trans) for activation of this receptor.

Restriction of W6.48 by a TMH6 aromatic cluster is not possible in the cannabinoid receptors, as the CB_1 receptor has leucines at 6.44, 6.51, and 6.52. Instead, the CB_1 receptor contains a microdomain of aromatic residues that face into the ligand-binding pocket in the TMH3-4-5-6 region, including F3.25(190), F3.36(201), W4.64(256), Y5.39(276), W5.43(280), and W6.48(357) (Fig. 2). In work reported here, we suggest that the F3.36(201)/W6.48(357) interaction may act as a mimic of the 11-*cis*-retinal/W6.48 interaction in the Rho dark state and may serve as the "toggle switch" for CB_1 activation, with F3.36(201) χ_1 trans/W6.48(357) χ_1 g+ representing the inactive (R) and F3.36(201) χ_1 g+/W6.48(357) χ_1 trans representing the active (R*) state of CB_1. Modeling, mutation, and functional studies undertaken to test the importance of the TMH3-4-5-6 aromatic microdomain in ligand recognition and in the conformational changes that accompany activation of CB_1 suggest that a F3.36(201)/W6.48(357)-specific contact is an important constraint for the CB_1-inactive state.

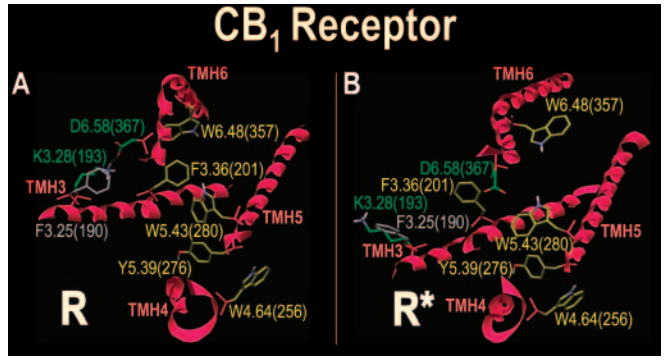

FIG. 2. **Models of the CB_1 R and R* states in the TMH3-4-5-6 region (in the absence of ligand) are illustrated here (1).** *A*, in the R state model, a salt bridge can form between K3.28(193) and D6.58 (367) (shown in *green*). F3.25(190) (shown in *gray*) is close enough to have a cation-π interaction with K3.28(193). A microdomain of clustered aromatic residues (shown in *yellow*) W6.48(357)/F3.36(201)/W5.43(280)/Y5.39(276)/W4.64(256) exists in the CB_1 TMH3-4-5-6 region. *B*, the conformational changes that occur upon receptor activation (R $\rightarrow$ R* transition) result in rotations of TMH3 and -6, as well as a change in the conformation of TMH6 (by moderation of its proline kink angle) (6–8, 10). The K3.28(193)-D6.58(367) salt bridge is broken (residues illustrated in *green*) and K3.28(193) and F3.25(190) (in *gray*) are now oriented toward the TMH2/7 region of CB_1. The aromatic cluster present in the inactive state model also undergoes re-arrangement, with W6.48(357)/W5.43(280)/Y5.39(276)/W4.64(256) (shown in *yellow*) maintaining an extended cluster, whereas F3.36(201) (*yellow*) is no longer part of this cluster.

EXPERIMENTAL PROCEDURES

Molecular Modeling

Amino Acid Numbering System—In the discussion of receptor residues below, the amino acid numbering scheme proposed by Ballesteros and Weinstein (17) is used. In this numbering system, the most highly conserved residue in each transmembrane helix (TMH) is assigned a locant of 0.50. This number is preceded by the TMH number and followed in parentheses by the sequence number. All other residues in a TMH are numbered relative to this residue. In this numbering system, for example, the most highly conserved residue in TMH2 of the mouse CB_1 receptor is D2.50(164). The residue that immediately precedes it is A2.49(163). Fig. 1 serves as a reference for this numbering system in mouse CB_1.

Definition of Rotameric State of χ_1—Different nomenclatures have been used to define the rotameric state of side chain torsion angles. The nomenclature employed here for the χ_1 torsion angle is that described by Shi *et al*. (16). When the heavy atom at the γ position is opposite to the backbone nitrogen when viewed from the β-carbon to the α-carbon, the χ_1 is defined to be trans. When the heavy atom at the γ position is opposite to the backbone carbon when viewed from the β-carbon to the α-carbon, the χ_1 is defined to be gauche+ (g+). When the heavy atom at the γ position is opposite to the α-hydrogen when viewed from the β-carbon to the α-carbon, the χ_1 is defined to be gauche− (g−). By using this nomenclature system, the side chain conformations discussed here are categorized into g− ($0° < \chi_1 < 120°$), trans ($120° < \chi_1 < 240°$), or g+ ($240° < \chi_1 < 360°$).

Conformational Memories Studies of TMH6 and the W6.48A Mutant TMH6—In order to explore the consequences of the W6.48A mutation upon the conformation of TMH6, we used the conformational memories (CM) method (18), a method that employs multiple Monte Carlo/simulated annealing random walks and the Amber* force field. Conformational memories has been shown to converge in a very practical number of steps and to be capable of overcoming energy barriers efficiently. By using CM, the conformational properties of a helix can be fully characterized by the free energy of each of the conformations that the helix can adopt, and this property includes not only the intrinsic energy of each conformational state but also the probability that the helix will adopt each particular conformation relative to all other ones accessible in an equilibrated thermodynamic ensemble.

The calculation is performed in two phases. In the first phase, repeated runs of Monte Carlo/simulated annealing are carried out to map the entire conformational space of the helix. In the second phase, new Monte Carlo/simulated annealing runs are performed only in the populated regions identified in the first phase of the calculation.

WT TMH6 Versus TMH6 W6.48A Mutant—The CB_1 TMH6 (from residue 6.30 to residue 6.57, DIRLAKTLVLILVVLIICWGPLLAIMVY) and the TMH6 W6.48A mutant (DIRLAKTLVLILVVLIIC**A**GPLLAIMVY) were built using MacroModel (19). In the Rho 2.8-Å crystal structure (3), χ_1 of W6.48 is g+. In order to be consistent with this result, χ_1 = g+, −60° was chosen as the starting conformation for W6.48(357) in the WT TMH6 run. Our previous CM studies of TMH6 have suggested that when C6.47(356) adopts a trans conformation (χ_1 = 180°) and forms a hydrogen bond with the backbone of TMH6, TMH6 exhibits its greatest flexibility. In the studies reported here, the χ_1 of C6.47(356) was set to trans. The χs for all other amino acids in TMH6 were left at the default values used by MacroModel when an α-helix is built (19). The charges on all charged residues in each TMH6 studied were reduced to one-third of their values to prevent artifacts during the CM runs.

All calculations were performed using a distance-dependent dielectric. Each TMH6 was first minimized using the Amber* forcefield in MacroModel (19). For WT CB_1 TMH6 73 torsion angles were allowed to vary during the CM runs, whereas 71 torsion angles were allowed to vary in the CB_1 TMH6 W6.48(357)A mutant run. These included all helix backbone ϕs and φs, as well as amino acid side chain torsion angles for L6.39(348) to I6.54(363) (excluding χ_1 dihedrals on β-branched residues and χ_2 on C6.47(356) in this span). The backbone ϕs and φs for I6.46(355) through P6.50(359) (*i.e.* the turn before P6.50(359)) were allowed to vary ±50° from their minimized values. All other backbone torsions were allowed to vary ± 10°. The χ_1 and χ_2 for W6.48(357) in WT TMH6 and the χ_1 for C6.47(356) (in both the WT and W6.48(357)A mutant runs) were allowed to vary ±60°. The χ_2 for C6.47(356) was not allowed to vary in either run. All other side chain torsion angles were allowed to vary ± 180° without constraints. The calculation was performed in two phases as indicated below.

Exploratory Phase—In the exploratory phase, a random walk was used to identify the region of conformational space that is populated for each torsion angle studied. Starting at a temperature of 2070 K, 20,000 steps were applied to the rotatable bonds with cooling in 18 steps to a final temperature of 310 K. Trial conformations were generated at each temperature by randomly picking three torsion angles from the set of 73 (71 in the W6.48A mutant) and changing each angle by a random value within the range set in the calculation (see above). After each step, the generated trial conformation was either accepted or rejected using the Metropolis criterion. This calculation was repeated for a total of 100 cycles. Accepted conformations were used to map the conformational space of TMH6 by creating "memories" of values for each torsion angle that were accepted.

Biased Annealing Phase—In the second phase of the CM calculation, the only torsion angle moves attempted were those that would keep the angle in the "populated conformational space" mapped in the exploratory phase. The biased annealing phase began at a temperature of 722 K cooling to 310 K in 8 steps. 100 structures were written out at 310 K.

Analysis of Output—Finally, the output of 100 structures at 310 K was clustered using X-Cluster in MacroModel (19). This program reorders the structures according to their root mean square deviation and groups the structures into families of similar conformers. The resulting 100 structures from CM were also analyzed using the program, ProKink (20). This program, which is embedded in the Simulaid Conversion program,[2] was used to calculate the face shift, wobble, and bend angles of each helix. Statistically significant differences between the face shift, wobble, and bend angles of the R and R* CB_1 WT *versus* W6.48A R and R* helix families were evaluated in the two-sample independent *t* test computed using OriginPro version 7 (Origin Lab Corp.).

Models of CB_1 R and R States*—In the present study, the literature on GPCR activation discussed above was used to generate an R* CB_1 TMH bundle from a model of the inactive (R) CB_1 receptor based on the 2.8-Å crystal structure of rhodopsin (3). The creation of these two forms of CB_1 is described briefly below.

Model of Inactive State (R) Form of CB_1—A model of the R form of CB_1 was created using the 2.8-Å crystal structure of bovine Rho (3). First, the sequence of the mouse CB_1 receptor (22) (see Fig. 1) was aligned with the sequence of bovine Rho using the same highly conserved residues as alignment guides that were used initially to generate our first model of CB_1 (23). TMH5 in CB_1 lacks the highly conserved proline in TMH5 of Rho. Therefore, the sequence of CB_1 in the TMH5 region was aligned with that of Rho as described previously using its hydrophobicity profile (23). The mouse CB_1 sequence (22) is 97.7% identical to the human CB_1 sequence (2) overall and 100% identical within the transmembrane regions. The mouse sequence is one residue longer (473 residues) than the human sequence (472 residues) due to an additional residue in the N terminus.

Initial helix ends for mouse CB_1 were chosen in analogy with those of Rho (3). With the exception of TMH1, these helix ends were found to be within one turn of the helix ends originally calculated by us and reported in 1995 (23). Two changes dictated by the CB_1 sequence were made in the helix ends. The shortness of the E1 loop region in CB_1 necessitated starting TMH3 at 3.23 (N3.23(188) to R3.56(221)). The break in helicity caused by the GWNC sequence motif on the extracellular end of TMH4 necessitated that TMH4 end at 4.62 instead of 4.66 (as is found in Rho). Changes to the general Rho structure that were necessitated by sequence divergences included the absence of helix-kinking proline residues in TMH1 and TMH5, the lack of a GG motif in TMH2, as well as the presence of extra flexibility in TMH6 (24). Our recent conformational memories study of TMH6 in CB_1 revealed that TMH6 in CB_1 has high flexibility due to the small size of residue 6.49 (a glycine) immediately preceding Pro 6.50. The conformer selected from our CM results for inclusion in the CB_1 R bundle (Pro kink angle = 53.1°) was chosen so that R3.50(215) and D6.30(339) could form a salt bridge at the intracellular ends of TMH3 and -6 in the CB_1 TMH bundle. An analogous salt bridge has been shown to be an important stabilizer of the inactive state of the β_2-adrenergic receptor, the 5HT-2a receptor (10), and to be present in Rho (3). Because of the extreme flexibility of TMH6 in CB_1, we have proposed that an additional TMH3–6 salt bridge, K3.28(193)–D6.58(367), stabilizes the inactive state on the extracellular side of the TMH bundle (25).

Model of Active (R) Form of CB_1*—Based upon experimental results for rhodopsin and the β_2-adrenergic receptor (6, 10, 15, 26), the R* (active) CB_1 bundle was created from the inactive (R) model of CB_1 by substituting a less kinked TMH6 (21.8° kink angle) from our CM results (25)for which the R3.50(215) and D6.30(339) salt bridge would be broken due to the movement of the intracellular end of TMH6 away from

[2] M. Mezei, personal communication.

TABLE I

Binding profile of wild type and mutant cell lines used in this study

The K_d and B_{max} values were obtained from saturation experiments using [^{3}H]CP55,940 performed on membranes prepared from wild type and mutant HEK cell lines as described previously (1). Inhibition constants (K_i) values were obtained from competitive binding experiments using the listed ligands *versus* [^{3}H]CP55,940 (1). Data are the means and corresponding 95% confidence limits of three independent experiments each performed in triplicate.

Cell line	CP55,940, K_d (nM)/B_{max}	WIN 55,212-2, K_i (nM)	Anandamide, K_i (μM)	SR141716A, K_i (nM)
	pmol/mg			
CB_1	1.5 (0.53–2.4)/4.4 (3.5–5.3)	12 (7.0–20)	0.3 (0.1–0.6)	4.8 (2.2–10)
F3.25(190)A	5.5 (0.3–10)/3.2 (1.9–4.5)	15 (3.7–49)	1.8[a] (0.6–5.6)	9.6 (4.6–20)
F3.36(201)A	2.3 (0.6–4.1)/5.2 (3.6–6.9)	107[a] (44–261)	0.3 (0.1–1.1)	14[a] (7.3–29)
W5.43(280)A	5.4 (1.2–9.5)/1.9[a] (1.1–2.6)	199[a] (43–914)	0.3 (0.2–0.7)	46%[a] displacement at 5 μM
W6.48(357)A	3.2 (2.0–4.4)/4.4 (3.8–5.2)	45[a] (22–92)	0.3 (0.1–0.5)	33[a] (23–45)

[a] Values indicate statistically significant differences from wild type ($p < 0.05$).

that of TMH3 and out into lipid (10). Rotations of both TMH3 and TMH6 were also central to the creation of the R* model. The details of these rotations are presented elsewhere (24).

Preparation of Helices—Each helix of the model was capped as the acetamide at its N terminus and as the *N*-methyl amide at its C terminus. Ionizable residues in the first turn of either end of the helix were neutralized, as were any lipid facing charged residues. Ionizable residues were considered charged if they appeared anywhere else in the helix.

Energy Minimization, Unoccupied Receptor States—The energy of the CB_1 R or CB_1 R* TMH bundle complex was minimized using the AMBER* united atom force field in Macromodel 6.5 (Schrödinger Inc., Portland, OR). A distance-dependent dielectric, 8.0-Å extended nonbonded cut-off (updated every 10 steps), 20.0-Å electrostatic cut-off, 4.0-Å hydrogen bond cut-off, and explicit hydrogens on sp^2 carbons were used. The first stage of the calculation consisted of 2000 steps of Polak-Ribier conjugate gradient (CG) minimization in which a force constant of 225 kJ/mol was used on the helix backbone atoms in order to hold the TMH backbones fixed, while permitting the side chains to relax. The second stage of the calculation consisted of 100 steps of CG in which the force constant on the helix backbone atoms was reduced to 50 kJ/mol in order to allow the helix backbones to adjust. Stages one and two were repeated with the number of CG steps in stage two incremented from 100 to 500 steps until a gradient of 0.001 kJ/(mol·Å^2) was reached. This same protocol was followed for the W6.48(357)A TMH bundle.

Assessment of Aromatic Stacking Interactions—Residues were designated here as participating in an aromatic stacking interaction if subject rings had centroid to centroid distances (d) between 4.5 and 7.0Å. These interactions were further classified as "tilted t" arrangements if $30° \leq \alpha \leq 90°$ and as parallel arrangements for $\alpha < 30°$ (where α is the angle between normal vectors of interacting rings) (27). Parallel arrangements were considered favorable only if the interacting rings were offset from each other (28). All measurements were made using MacroModel 8.1.

Assessment of Cation-π Interactions—In their study of cation-π interactions in the protein data bank, Gallivan and Dougherty (29) considered a cation-π interaction to be present in structures when both $r \leq 10$ Å and $r' \leq 10$ Å, where r is the distance between the ammonium nitrogen (NZ) of the protonated residue and the aromatic ring centroid, and r' is the distance between CE of the protonated residue (in the case here, a Lys) and the aromatic ring centroid (29). However, these investigators reported that in 88% of the cation-π interactions considered, $r < 5$ Å and $r' < 5$ Å. A cation-π interaction was judged to be present in the work presented here if $r < 5$ Å and $r' < 5$ Å. The r and r' distances were measured here using MacroModel 8.1.

Ligand Conformations and Docking Positions—The binding site conformations and anchoring interactions inside the receptor used for each ligand discussed here are based on our recently published work (1).

Mutation Studies

Materials—SR141716A and CP55,940 were obtained from the National Institute on Drug Abuse. WIN 55,212-2 was purchased from RBI (Natick, MA), and anandamide was purchased from Tocris (Ellisville, MI).

Mutagenesis, Cell Culture, and Radioligand Binding—The cell lines used in this study have been described previously (1). Site-directed mutations were introduced into mouse CB_1 in pcDNA3 at the designated sites using the QuikChange mutagenesis technique (Stratagene, La Jolla, CA). Stable cell lines were created by transfection of wild type or mutant CB_1pcDNA3 into HEK 293 cells by the LipofectAMINE reagent (Invitrogen) and cultured as described previously (30). Cell lines containing moderate to high levels of receptor mRNA, assessed by Northern analysis, were tested for receptor binding and signal transduction properties. Receptor binding was determined as described previously (1). Cell lines with the most similar receptor expression profile, as ascertained by B_{max} values, were chosen for further analysis (Table I).

[^{35}S]GTPγS Binding Assay—The basal activity and the ability of various cannabinoids to stimulate the wild type CB_1 receptor or the mutant receptors were tested with [^{35}S]GTPγS binding. Cells were harvested in phosphate-buffered saline containing 1 mM EDTA and centrifuged at 500 × g for 5 min. The cell pellet was homogenized and centrifuged at 50,000 × g for 10 min at 4 °C. The pellet was resuspended in buffer composed of (mM): Tris-HCl 50, EDTA 1, and $MgCl_2$ 3, pH 7.4, to yield protein concentration of 2–4 mg/ml. Membrane preparations were aliquoted and stored at −80 °C. Binding was initiated by the addition of 20 μg of membrane protein into glass tubes containing 0.1 nM [^{35}S]GTPγS, 10 μM GDP in GTPγS binding buffer (50 mM Tris-HCl, 100 mM NaCl, 3 mM $MgCl_2$, 0.2 mM EGTA, 0.1% bovine serum albumin, pH 7.4). Nonspecific binding was assessed in the presence of 20 μM unlabeled GTPγS. Binding assays were performed for 90 min at 30 °C with various concentrations of WIN 55212-2, CP55,940, anandamide, and SR141716A in a total volume of 500 μl. Free and bound radioligands were separated by a rapid filtration through Whatman GF/C filters. Filters were shaken for 1 h in 6 ml of scintillation fluid (Fisher), and radioactivity was determined by a liquid scintillation counter.

Expression in Oocytes and Recordings—This technique was performed as described previously (31). Briefly, 0.013 pg of GIRK1 and GIRK4 and 25 ng of CB_1 (wild type or mutant) cRNAs were co-injected using a micromanipulator (Drummond Scientific Co., Broomall, PA) into *Xenopus laevis* oocytes (*Xenopus* One, Dexter, MI). Recordings were performed after 7–9 days of incubation in 0.5× L-15 media (Sigma) supplemented with L-glutamine and antibiotics. For recordings, the eggs were placed in a chamber (total volume 200 ml) and perfused at 4 ml/min with LK (2 mM KCl, 96 mM NaCl, 2 mM $CaCl_2$, 1.8 mM $MgCl_2$, and 5 mM HEPES, pH 7.5), HK (96 mM KCl, 2 mM NaCl, 2 mM $CaCl_2$, 1.8 mM $MgCl_2$, and 5 mM HEPES, pH 7.5), or HK plus drug. Bovine serum albumin (3 μM) was added to all drug solutions to minimize absorption of cannabinoid compounds to the perfusion system. Oocytes were impaled with two microelectrodes filled with 3 M KCl and were voltage-clamped at reported voltages using an Axon GeneClamp amplifier (Axon Instruments, Foster City, CA). Currents were filtered at 10 Hz, collected, and analyzed using a Macintosh Centris 650 containing a 16-bit analog-digital interface board and voltage-clamp software running under the IGOR graphics environment (Wavemetrics, Lake Oswego, OR). Oocytes were voltage clamped at −80 mV and superfused in a low potassium (LK) solution containing 96 mM Na^+ and 2 mM K^+. When a high potassium (HK) solution containing 96 mM K^+ and 2 mM Na^+ was exchanged for LK, an inward current was produced and termed I_{HK}. I_{HK} represents the basal activity of GIRK1/4 channels. This current reached a plateau with ~30 s (31). At this point application of the cannabinoid agonists (WIN 55,212-2 or anandamide) in HK further enhanced the inward current. This agonist-induced current was named I_{Ag}. Concentration-response curves were generated by nonlinear regression of log percent concentration enhancement data ($I_{Ag}/I_{HK} \times 100$) with the use of the GraphPad Prism program (GraphPad, San Diego, CA).

Statistical Analyses—The EC_{50} and E_{max} values were calculated by unweighted least squares nonlinear regression of log concentration values *versus* percent effect. Significant differences were determined (GraphPad Prism) using analysis of variance or the unpaired Student's t test, where

suitable. Bonferroni-Dunn post-hoc analyses were conducted when appropriate. p values <0.05 defined statistical significance.

RESULTS

The TMH3-4-5-6 Aromatic Microdomain at the CB_1 Receptor; Comparison of R and R State Models in the Absence of Ligand*

CB_1 R State—Fig. 2*A* illustrates key features of the CB_1 TMH bundle model in the inactive (R) state in the TMH3-4-5-6 region. One of the significant features of this model is a salt bridge between K3.28(193) and D6.58(367) (N-O distance = 2.6 Å; N-H-O angle = 159°) (51). This salt bridge is made possible by the profound flexibility in TMH6 due to the presence of G6.49 in the CW*X*P motif of TMH6 (25). The TMH3-4-5-6 region of the R bundle in the absence of ligand is characterized by a W6.48(357)/F3.36(201)/W5.43(280)/Y5.39(276)/W4.64(256) aromatic cluster in which W6.48(357) stacks with F3.36(201) (d = 5.3 Å, α = 90°), whereas F3.36(201) stacks with W5.43(280) (d = 5.6 Å, α = 40°). W5.43(280) also has an off-set parallel stack with Y5.39(276) (d = 5.9 Å, α = 0°), whereas Y5.39(276) stacks with W4.64(256) (d = 6.5 Å, α = 90°) (see "Experimental Procedures" for definitions of d and α).

Residue 3.25 (190) does not stack with the other aromatic residues in the TMH3-4-5-6 region but still appears to be an important residue. In the R bundle, F3.25(190) is located directly extracellular to K3.28 and is close enough to K3.28 to be able to form a cation-π interaction with K3.28 (193) (NZ-centroid distance, r = 3.1 Å, CE-centroid distance, r' = 4.9 Å; see "Experimental Procedures" for definitions of distances). In the R state, the χ_1 for K3.28 (193) and for F3.25(190) is trans.

CB_1 R State*—Fig. 2*B* illustrates key features of the CB_1 TMH bundle model in the active (R*) state in the TMH3-4-5-6 region. The conformational changes that occur upon receptor activation result in rotations of TMH3 and -6 as well as a change in the conformation of TMH6 (by moderation of its proline kink angle) (6–8, 10). In our models, both W6.48(357) and F3.36(201) undergo a change in their χ_1 values from R to R*. χ_1 in W6.48(357) changes from g+ to trans and χ_1 of F3.36(201) changes from trans to g+ (see "Experimental Procedures" for definition of χ_1). In the R* TMH bundle, the K3.28(193) and D6.58(367) salt bridge is broken (N-O distance = 16.8 Å) because TMH3 and -6 rotate (counterclockwise from extracellular view) during the R to R* transition (*i.e.* activation) (26, 32). K3.28(193) has rotated away from D6.58(367) toward TMH2/TMH7, and D6.58(367) has rotated toward the TMH5–6 interface and is raised higher above the ligand-binding pocket due to the moderation of the TMH6 proline kink angle. The W6.48(357)/F3.36(201)/W5.43(280)/Y5.39(276)/W4.64(256) aromatic cluster present in the inactive state in the absence of ligand also undergoes rearrangement, with F3.36(201) no longer part of this cluster. In the TMH3-4-5-6 region of R* in the absence of ligand, W6.48(357) and W5.43(280) form an off-set parallel aromatic stacking interaction with each other (d = 4.9 Å, α = 30°). W5.43(280) also stacks with Y5.39 (d = 6.6 Å, α = 60°), whereasY5.39 stacks with W4.64 (d = 5.7 Å, α = 90°). This series of aromatic stacking interactions results in a large aromatic stack in R* comprised of W6.48(357)/W5.43(280)/Y5.39(276)/W4.64(256). F3.36(201) (χ_1 = g+) is not located near another TMH3-4-5-6 aromatic residue in the R* bundle, instead F3.36(201) is bounded by V3.40(205), V3.32(197), and L6.44(353).

As stated above, in the R* state, the rotation of TMH3 upon activation causes K3.28(193) to point toward TMH2/TMH7, and because F3.25(190) is one turn above K3.28(193), it also now faces the TMH2/TMH7 region. The χ1 for both K3.28(193) and F3.25(190) is g+ in the R* bundle.

Ligand Binding

We have recently published mutation and modeling studies of the CB_1 TMH3-4-5-6 aromatic microdomain in which binding sites for the inverse agonist SR141716A and the CB_1 agonists WIN 55212-2 and anandamide were identified (1).

Functional Analysis of Mutant Receptors

We have shown previously that the aromatic residues F3.36(201), W5.43(280), and W6.48(357) form specific interaction sites in CB_1 for aminoalkylindole agonist (WIN 55,212-2) and diaryl pyrazole inverse agonist/antagonist (SR141716A) ligands but not for endogenous (anandamide) and bicyclic cannabinoid (CP55,940) agonists (1). When the aromatic residues were individually mutated to alanine, a significant reduction in ligand binding affinity was only observed in the presence of WIN 55,212-2 and SR141716A but not CP55,940 and anandamide. The study presented here is a detailed functional analysis of these mutant receptors using two different cellular backgrounds. The mutants were studied in stable cell lines created in HEK cells or in oocytes where the mutant proteins were expressed transiently. The mutations were analyzed in two ways. Direct receptor-G protein stimulation in HEK cells was assessed using [^{35}S]GTPγS binding, and G protein stimulation downstream of the receptor was evaluated by measuring enhancement of GIRK channel activity in oocytes.

F3.36A(201)—The F3.36A(201) mutation produced a significant reduction in agonist-dependent activation produced by WIN 55,212-2 (Fig. 3, *A* and *B*, and Tables II and III). This could be observed at the level of direct receptor-G protein stimulation (GTPγS), and this outcome was even more profound downstream at GIRK1/4 channels. The affinity of WIN 55,212-2 at F3.36A(201) was reduced 8.9-fold in HEK cells, whereas the affinity of CP55,940 and anandamide was unaffected (1). Even the addition of high concentrations of WIN 55,212-2 could not produce substantial receptor activation suggesting the loss of affinity for the ligand, produced by the mutation, was not solely responsible for decreased activation. To strengthen this conclusion further, CP55,940 and anandamide were also tested because the mutation to alanine at F3.36(201) had no effect on the affinity of these ligands for the receptor (Table I). Full receptor activation could also not be produced with CP55,940 (see Fig. 3*D* and Table II) or with anandamide (see Fig. 3*C* and Table III).

We next examined whether observed reductions in function were the result of a constitutively activated receptor. The CB_1 receptor has been shown to have a high level of agonist-independent activation (*i.e.* constitutive activity) in transfected cell lines where the reporter system is a G protein-activated ion channel or an intracellular kinase (33, 34). The ability of CB_1 to activate G proteins in the absence of exogenously applied agonist has also been shown for native CB_1 receptors in human and rat brain (35, 36). Kearn and co-workers (37) have estimated that in WT CB_1, the receptor populations are 70% inactive state (R) and 30% active state (R*).

Agonist-independent activation of GPCRs can be assessed by measuring basal turnover of [^{35}S]GTPγS in transfected cells and by comparing the I_{HK} of GIRK1/4 in injected oocytes (38, 39). Consistent with previous findings (39), we found a 56% increase (WT CB_1 = 1055 ± 58 dpm, untransfected = 675* ± 73 dpm) in agonist-independent activation of [^{35}S]GTPγS in HEK cells expressing WT CB_1 compared with untransfected cells (Fig. 7 and Table IV). When the agonist-independent GTPγS activity of F3.36A(201) was compared with WT CB_1, a 73% increase (F3.36(201)A = 1825 ± 138 dpm, WT CB_1 = 1055 ± 58 dpm) was observed with the mutant (Fig. 7 and Table IV). A 62% increase was also observed when I_{HK} or basal

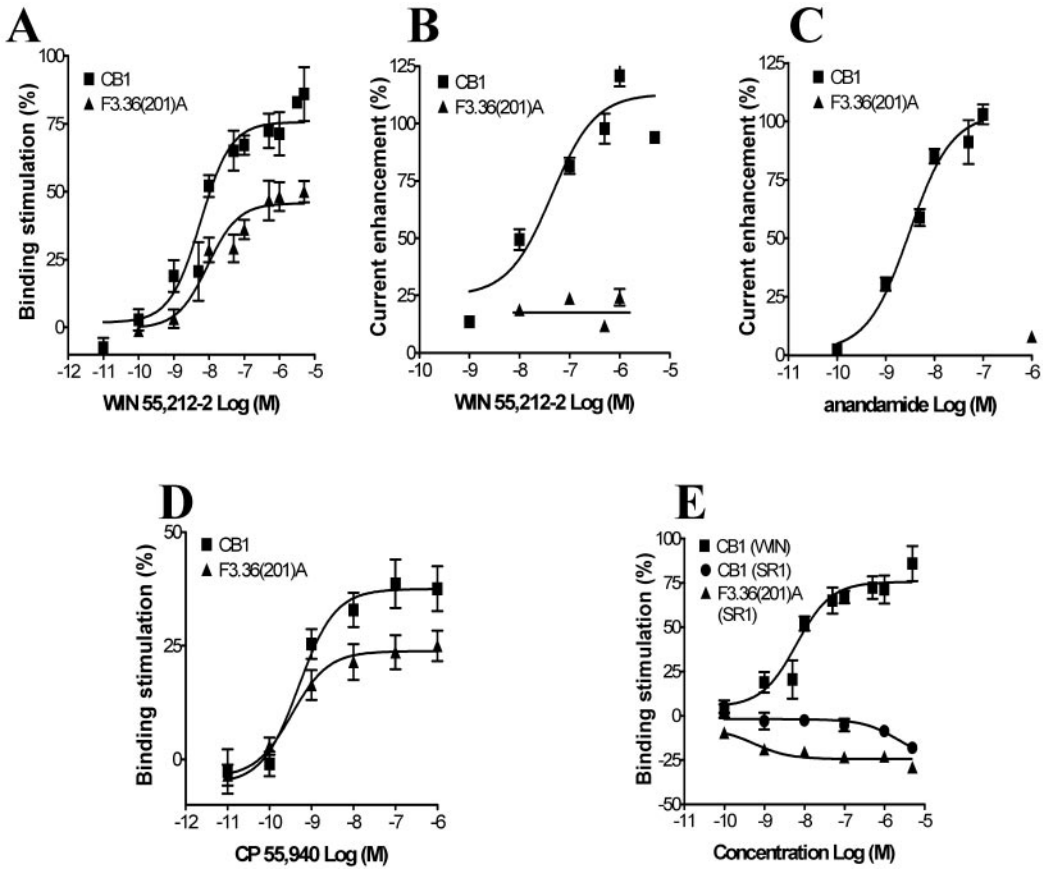

FIG. 3. **Comparison of WT CB_1 (■) and F3.36(201)A (▲) receptor activation.** WIN 55,212-2 (*A*), CP55,940 (*D*), and SR141716A (*E*) were used for concentration-response analysis of [^{35}S]GTPγS binding in HEK cell membranes expressing wild type or mutant receptor protein. ● represents the WT CB_1 response to SR141716A. Each data point shown is the mean ± S.E. of at least three independent experiments performed in triplicate. WIN 55,212-2 (*B*) and anandamide (*C*) were also used for concentration-response analysis in oocytes co-expressing GIRK1/4 and CB_1 (WT or mutant) cRNAs. The amount of RNA injected and the recording protocol are described under the "Experimental Procedures." Each data point in the concentration-response curve is the mean ± S.E. of 4–15 determinations made from at least two batches of oocytes.

TABLE II

Cannabinoid agonist stimulation of [^{35}S]GTPγS from membranes prepared from wild type and mutant cell lines

Data shown are the means ± S.E. of at least three experiments performed in triplicate.

Agonist	Cell line	EC_{50}	E_{max}
		nM	%
WIN 55,212-2	CB_1	5.3 (2.8–10)	76 (69–82)
	F3.25(190)A	33[a] (21–53)	74 (68–80)
	F3.36(201)A	9.3 (3.2–26)	45[a] (41–51)
	W5.43(280)A	1,300[a] (309–5,521)	81 (40–121)
	W6.48(357)A	61[a] (40–94)	147[a] (133–162)
CP55,940	CB_1	0.5 (0.2–1.5)	38 (32–43)
	F3.36(201)A	0.3 (0.1–0.6)	24[a] (21–26)
	W5.43(280)A	33[a] (5.9–85)	53 (34–71)
	W6.48(357)A	1.3 (0.8–2.2)	100[a] (94–107)

[a] Values indicate statistically significant differences from wild type ($p < 0.05$).

activity of GIRK1/4 was evaluated between F3.36A(201) and WT CB_1 (Fig. 8 and Table IV). Although the amount of receptor expressed in oocytes used for the GIRK assay cannot be determined, the B_{max} values for the WT and F3.36(201)A cell lines used for the GTPγS assay were not statistically different from one another (WT CB_1 B_{max} = 4.4 (3.5–5.3) pmol/mg; F3.36(201)A-B_{max} = 5.2 (3.6–6.9) pmol/mg; Table I). Thus, the 73% increase (relative to WT) in the level of GTPγS binding seen in the HEK cells stably transfected with F3.36(201)A cannot be attributed to an overexpression of mutant receptor protein (Table I). These combined data strongly suggested the F3.36A(201) mutant receptor had even greater constitutive activity than WT CB_1. To further support this hypothesis, the properties of the mutant receptor were evaluated using the CB_1-selective inverse agonist SR141716A. An inverse agonist should reduce the basal activity of the constitutively activated mutant receptor because the inverse agonist will force the receptor to adopt an inactive conformation; this was the case (Figs. 3*E* and 7). Furthermore, compared with WT CB_1 the inverse agonist response of SR141716A at F3.36A(201) was significantly increased (Fig. 3*E*). No inverse agonism was produced at WT CB_1 except at the highest (5 μM) concentration (17 ± 2%, n = 3) (Fig. 3*E*). However, inhibition of GTPγS binding occurred with F3.36(201)A in the presence of nanomolar concentrations of SR141716A with EC_{50} and E_{max} values of 0.6 (0.1–3.2) nM and −24 (−30 to −18) %, respectively.

Modeling studies also suggest that the F3.36(201)A mutant should be constitutively active, if it is assumed that changes in

TABLE III

Cannabinoid agonist stimulation of GIRK1/4 currents in oocytes expressing wild type and mutant CB_1 proteins

The amount of RNA injected and the recording protocol are described under "Experimental Procedures." Each data point in the concentration-response curve is the mean ± S.E. of 4–15 determinations made from at least two batches of oocytes.

Agonist	Cell line	EC_{50} ()	E_{max}
		nM	%
WIN 55,212-2	WT CB_1	13 (4–47)	127 (106–148)
	F3.25(190)A	25 (11–61)	116 (101–132)
	F3.36(201)A		24[a] (±8) at 1 μM
	W5.43(280)A	218[a] (66–723)	129 (93–165)
	W6.48(357)A	23 (12–44)	121 (104–137)
Anandamide	WT CB_1	3 (2–5)	93 (90–115)
	F3.25(190)A	47[a] (30–75)	59[a] (41–76)
	F3.36(201)A		8[a] (±0.5) at 1 μM
	W5.43(280)A	13[a] (6–36)	58[a] (48–73)
	W6.48(357)A	5 (2–16)	114 (101–127)

[a] Values indicate statistically significant differences from wild type ($p < 0.05$).

TABLE IV

Agonist-independent activation (or basal activity) of WT CB_1 and mutant receptors assessed by measuring basal turnover of [^{35}S]GTPγS binding or the I_{HK} of GIRK1/4

(SR) indicates reduction of basal [^{35}S]GTPγS binding in the presence of 1 μM SR141716A. [^{35}S]GTPγS binding data shown are the mean ± S.E. of at least three experiments performed in triplicate. To determine basal potassium channel activity or I_{HK}, a large number of oocytes (n = 20–46) were analyzed for each condition from at least two batches of oocytes.

Measure	Cell line	dpm
Basal [^{35}S]GTPγS	WT CB_1	1055 ± 58
	Untransfected HEK	675[a] ± 73
	F3.25(190)A	1114 ± 55
	F3.36(201)A	1825[a] ± 138
	F3.36(201)A (SR)	1042 ± 69
	W5.43(280)A	891 ± 45
	W6.48(357)A	1263 ± 12
	Cell line	I_{HK}
		μA
I_{HK} of GIRK1/4	WT CB_1	0.74 ± 0.12
	F3.25(190)A	0.87 ± 0.12
	F3.36(201)A	1.2[a] ± 0.09
	W5.43(280)A	0.92 ± 0.14
	W6.48(357)A	0.79 ± 0.09

[a] Values indicate statistically significant differences from wild type ($p < 0.05$).

the TMH3-4-5-6 aromatic cluster influence the state preference for the receptor. The loss of aromaticity at 3.36 (*i.e.* in the F3.36(201)A mutation) would result in the inability of W6.48(357) to participate in the extended aromatic cluster to which it belongs in WT CB_1. Specifically, this mutation would reduce the aromatic cluster present in the R state of WT CB_1 from W6.48(357)/F3.36(201)W5.43(280)/Y5.39(276)/W4.64(256) to W5.43(280)/Y5.39(276)/W4.64(256) (Fig. 2*A*). However, the F3.36(201)A mutation would not have an effect on the R* state, as F3.36(201) is not part of the aromatic cluster in the R* state of CB_1 (Fig. 2*B*). Thus, the W6.48(357)/W5.43(280)/Y5.39(276)/W4.64(256) cluster present in the R* state would be unchanged by the F3.36(201)A mutation. The net result of the F3.36(201)A mutation, therefore, should be a de-stabilization of the inactive state of CB_1, leading to increased constitutive activity.

W5.43(280)A—The EC_{50} values reported in Tables II and III show that the potency of WIN 55,212-2 at the W5.43(280)A mutant was reduced 245- and 16.8-fold when this receptor was studied by using GTPγS binding or by measuring enhancement of GIRK channel activity, respectively (Fig. 4, *A* and *B* and Tables II and III).

The full effect of WIN 55,212-2, however, at the W5.43(280)A mutant receptor could be achieved at higher concentrations. The substantial reductions in potency, in two cell systems, may be due in part to the decreased affinity of WIN 55,212-2 at W5.43(280)A. The affinity of WIN 55,212-2 at W5.43(280)A was reduced 16.8-fold in HEK cells, whereas the affinity of CP55,940 and anandamide was unaffected (Table I) (1). Because the affinities of CP55,940 and anandamide were unaffected at this mutation, the functional responses produced by these ligands were tested at W5.43(280)A to determine whether the effects observed in the presence of WIN 55,212-2 were primarily a result of a reduction in affinity at the mutant receptor. As shown in Fig. 4, *C* and *D*, there was a substantial reduction in the potency of both anandamide and CP55,940 at W5.43(280)A. It is clear in Table I, however, that the B_{max} of the W5.43(280)A mutant was statistically lower than that of WT CB_1. Lower receptor expression levels can produce a rightward shift in plots of response *versus* log[ligand] compared with a system in which a greater amount of receptor protein is expressed, despite the fact that the ligand has equal affinity in both systems. Thus, the reduced expression level of the W5.43(280)A mutant compared with WT CB_1 may explain the rightward shifts in Fig. 4, *C* and *D,* seen for anandamide and CP55940 (40). There were no significant changes in agonist-independent activation of W5.43(280)A in either cell system tested (Figs. 7 and 8 and Table IV).

W6.48A(357)—The EC_{50} values reported in Tables II and III show that the potency of WIN 55,212-2 at the W6.48(357)A mutant was reduced 12- and 1.8-fold when this receptor was studied using GTPγS binding or by measuring enhancement of GIRK channel activity, respectively (Fig. 5, *A* and *B*, and Tables II and III). However, the loss of potency observed with GIRK channel activity was not significant. The effects on potency may be due to the decreased affinity of WIN 55,212-2 at W6.48(357)A. The affinity of WIN 55,212-2 at W6.48(357)A was reduced 3.8-fold in HEK cells, whereas the affinity of CP55,940 and anandamide was unaffected (Table I) (1). Because the affinity of CP55,940 and anandamide was unaffected at this mutation, the functional responses produced by these ligands were tested at W6.48A(357). As shown in Fig. 5, *C* and *D*, and Tables II and III, there was no significant reduction in the potency of either CP55,940 or anandamide at W6.48A(357). These data suggest the loss in potency observed for WIN 55,212-2 stimulation of GTPγS binding at W6.48(357)A was the result of the selective loss of affinity for WIN 55,212-2 at this mutant receptor. It should be noted that a comparison of the shifts in potency for WIN 55,212-2 at both W6.48(357)A and W5.43(280)A demonstrate the GTPγS assay is more sensitive to this observable effect compared with studying GIRK channel activity (Figs. 4, *A* and *B* and Fig. 5, *A* and *B*, and Tables II and III).

Most interestingly, the maximum stimulation of GTPγS activity produced by WIN 55,212-2 at W6.48(357)A was signifi-

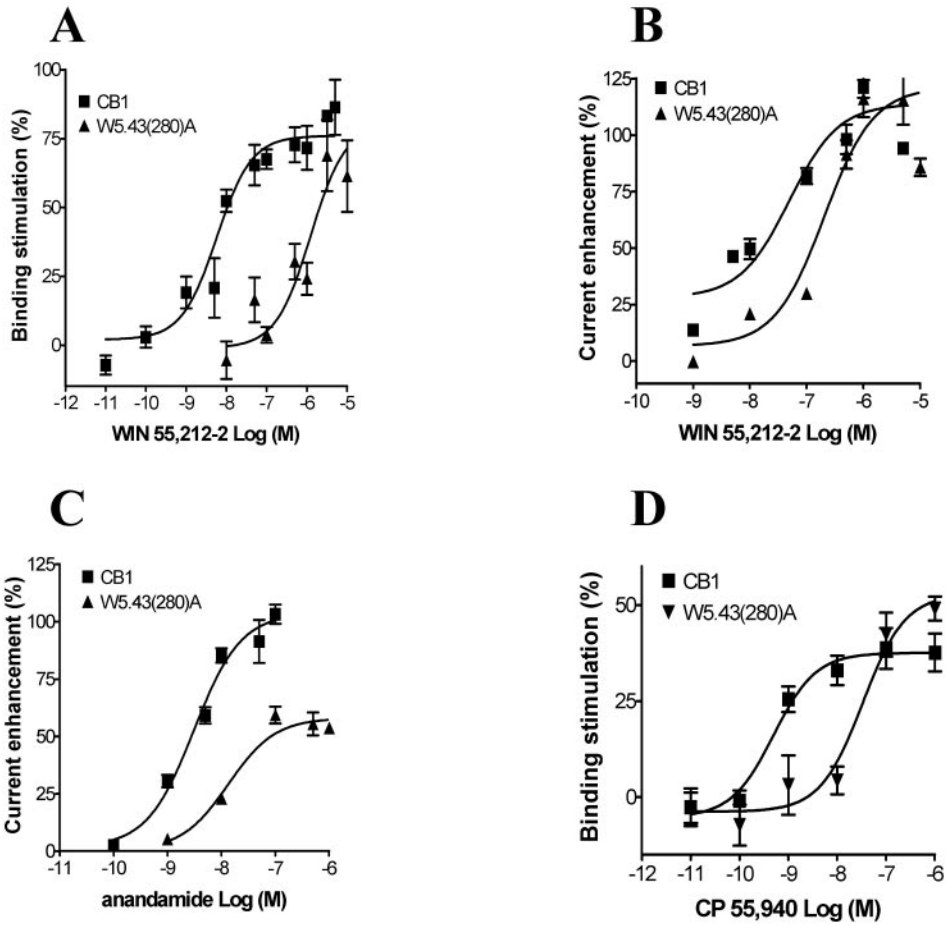

FIG. 4. **Comparison of WT (■) CB_1 and W5.43(280)A (▲) receptor activation.** WIN 55,212-2 (*A*) and CP55,940 (*D*) were used for concentration-response analysis of [^{35}S]GTPγS binding in HEK cell membranes expressing wild type or mutant receptor protein. Each data point shown is the mean ± S.E. of at least three independent experiments performed in triplicate. WIN 55,212-2 (*B*) and anandamide (*C*) were also used for concentration-response analysis in oocytes co-expressing GIRK1/4 and CB_1 (WT or mutant) cRNAs. The amount of RNA injected and the recording protocol are described under the "Experimental Procedures." Each data point in the concentration-response curve is the mean ± S.E. of 4–15 determinations made from at least two batches of oocytes.

cantly enhanced compared with WT CB_1 (Fig. 5*A* and Table II). To determine whether this effect was specific for aminoalkylindoles, the bicyclic cannabinoid CP55,940 was also tested at W6.48(357)A. As observed with WIN 55,212-2, CP55,940 also produced enhanced stimulation of GTPγS activity at W6.48(357)A compared with WT CB_1 (Fig. 5*D*). The enhanced activity of WIN 55,212-2 at W6.48(357)A was not observed when GIRK channel activity was measured (Fig. 5*B*).

There were no significant changes in agonist-independent activation of W6.48(357)A in either cell system tested (Figs. 7 and 8 and Table IV). Consistent with unchanged constitutive activity, the response to the inverse agonist at W6.48(357)A was not different from the response of WT CB_1 to the inverse agonist (Fig. 5*E*). Modeling studies also suggest that the W6.48(357)A mutant should not be constitutively active, if it is assumed that changes in the TMH3-4-5-6 aromatic cluster influence the state preference for the receptor. The W6.48A mutation will affect the TMH3-4-5-6 aromatic cluster in both the R and R* states. In the R state, the W6.48A mutation will result in the loss of one aromatic stacking interaction, *i.e.* the W6.48(357)/F3.36(201)/W5.43(280)/Y5.39(276)/W4.64(256) cluster in R will become a F3.36(201)/W5.43(280)/Y5.39(276)/W4.64(256) cluster in the mutant. In the R* state, the W6.48(357)/W5.43(280)/Y5.39(276)/W4.64(256) cluster present in the R* state will become a W5.43(280)/Y5.39(276)/W4.64(256) cluster in the mutant. Because aromatic stacking in both the R and R* states will be equally impacted, it is reasonable to expect that the W6.48A mutant will not produce a change in basal levels for the W6.48A mutant relative to WT CB_1, and this is what was seen experimentally.

F3.25(190)A—We previously reported that F3.25(190) is not part of the binding site of WIN 55,212-2, SR141716A, or CP55,940 but is a part of the anandamide-binding pocket (1). When F3.25(190) was mutated to an alanine, a 6-fold reduction in binding affinity was observed in the presence of anandamide, but no changes were observed in the presence of WIN 55,212-2, SR141716A, and CP55,940 (Table I). When GIRK channel activity was measured there was a significant reduction in both the potency and efficacy of anandamide at F3.25(190)A but no change in the presence of WIN 55,212-2 (Fig. 6, *A* and *B,* and Table III).

This result correlates with the binding data and receptor modeling. The effect seen with anandamide is likely to be related in part to the decreased affinity of anandamide for the F3.25(190)A mutant, as F3.25(190) is part of the anandamide-binding site (1). Anandamide stimulation of GTPγS turnover, in HEK cells transfected with F3.25(190)A, could not be measured because the partial agonist nature of the endogenous ligand results in a nonsignificant amount of GTPγS stimulation (41). Therefore, the findings with anandamide and the GIRK channel activity could not be compared with GTPγS stimulation because anandamide did not produce a significant functional response in HEK cells. There was a 6.2-fold decrease

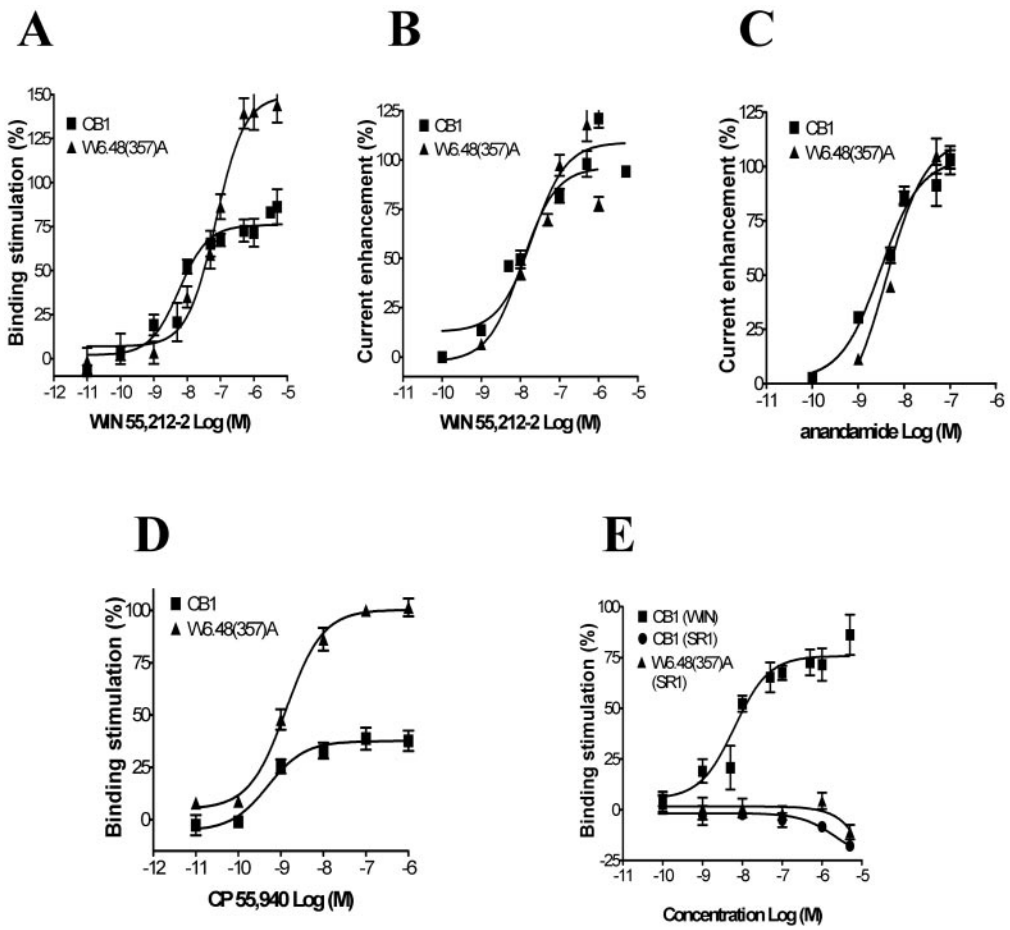

FIG. 5. **Comparison of WT (■) CB_1 and (▲) W6.48(357)A receptor activation.** WIN 55,212-2 (*A*), CP55,940 (*D*), and SR141716A (*E*) were used for concentration-response analysis of [^{35}S]GTPγS binding in HEK cell membranes expressing wild type or mutant receptor protein. ● represents the WT CB_1 response to SR141716A. Each data point shown is the mean ± S.E. of at least three independent experiments performed in triplicate. WIN 55,212-2 (*B*) and anandamide (*C*) were used for concentration-response analysis in oocytes co-expressing GIRK1/4 and CB_1 (WT or mutant) cRNAs. The amount of RNA injected and the recording protocol are described under the "Experimental Procedures." Each data point in the concentration-response curve is the mean ± S.E. of 4–15 determinations made from at least two batches of oocytes.

in the potency of WIN 55,212-2 when receptor activation was assessed by measuring GTPγS activity.

These agonists do not exhibit affinity changes from WT in the F3.25(190)A mutant. However, the effects observed on potency and/or efficacy reported here for WIN 55212-2 at the F3.25(190)A mutant may be related to the general role F3.25(190) plays in positioning K3.28 in the TMH bundle. As is clear from Fig. 2, F3.25(190) is just above K3.28 in the inactive state of CB_1 and has a cation-π interaction ($r \leq 5$ Å) with this residue. Gallivan and Dougherty (29) have reported that 14.5% of all cation-π interactions found in the "Protein Data Bank Select" list of Sander and co-workers (42, 43) represent such Lys-Phe interactions. Our modeling studies suggest that these residues move in concert with each other, as they both have trans χ_1s in the R state and g+ χ_1s in the R* state. F3.25(190) may act as a chaperone of K3.28 to position it in the correct location in R* for ligand interaction and to shield it from the extracellular milieu in the R state. Because residue positions in TMH3 R* may be changed in the absence of aromaticity at position 3.25, it is possible that ligands that do not bind to F3.25(190) can have their potency and/or efficacy affected by the F3.25(190)A mutation.

There were no significant changes in agonist-independent activation of F3.25(190)A in either cell system tested (Fig. 7 and Fig. 8 and Table IV). F3.25(190) is not part of the TMH3-4-5-6 aromatic cluster that characterizes the R and R* states of CB_1 (see Fig. 2). Therefore, the mutation of this aromatic residue to a nonaromatic residue would not be expected to affect basal levels.

Toggle Switch Residues

Fig. 9 illustrates the relationship between F3.36(201) and W6.48(357)in the R and R* states of CB_1. In the context of the inactive state model (see Fig. 9, *left*), F3.36(201) (χ_1 = trans) is located opposite W6.48(357)(χ_1 = g+) and has an aromatic stacking interaction with W6.48(357) that would prevent the χ_1 of W6.48(357) from changing from g+ to trans, thus stabilizing TMH6 in its inactive conformation. In the active state of CB_1, F3.36(201) and W6.48(357) change conformations (F3.36(201)(χ_1 = trans)/W6.48(357)(χ_1 = g+) → F3.36(201)(χ_1 = g+)/W6.48(χ1 = trans)) in order to rotate past each other and F3.36(201) (χ_1 = g+) and W6.48(357) (χ_1 = trans) are located too far apart in R* to interact with each other (see Fig. 9, *right*).

Conformational Memories Study of WT TMH6 Versus W6.48A TMH6—TMH6 in the class A GPCRs contains the highly conserved sequence motif, CW*X*P. This proline containing region of TMH6 is thought to act as a flexible hinge during GPCR activation (44). Proline residues are known to perturb the structure of helices by introducing a kink between the segments preceding (pre-proline helix) and following the proline residue (post-proline helix). The distortion of the helical structure results from the avoided steric clash between the ring of the proline at position (*i*) and the backbone carbonyl at position (i − 4), as well as the elimination of helix backbone

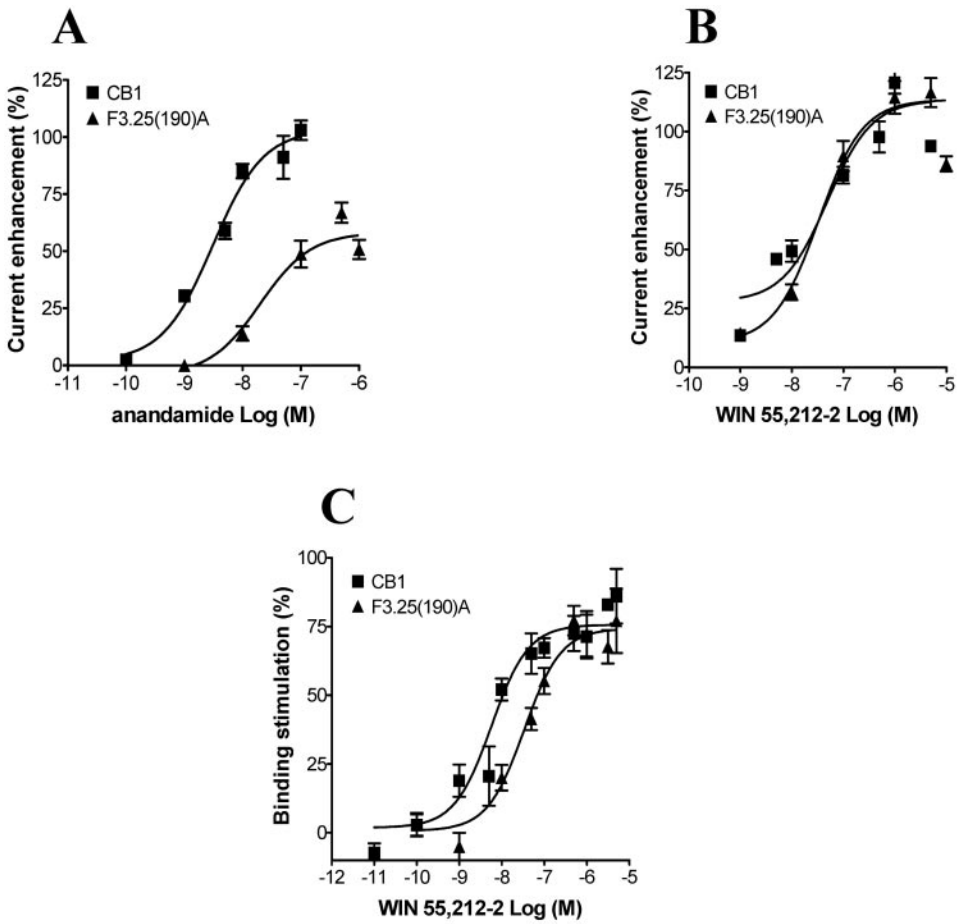

FIG. 6. **Comparison of WT (■) CB_1 and F3.25(190)A (▲) receptor activation.** Anandamide (*A*) and WIN 55,212-2 (*B*) were used for concentration-response analysis in oocytes co-expressing GIRK1/4 and CB_1 (WT or mutant) cRNAs. The amount of RNA injected and the recording protocol are described under the "Experimental Procedures." Each data point in the concentration-response curve is the mean ± S.E. of 4–15 determinations made from at least two batches of oocytes. *C*, WIN 55,212-2 was used for concentration-response analysis of [^{35}S]GTPγS binding in HEK cell membranes expressing wild type or mutant receptor protein. Each data point shown is the mean ± S.E. of at least three independent experiments performed in triplicate.

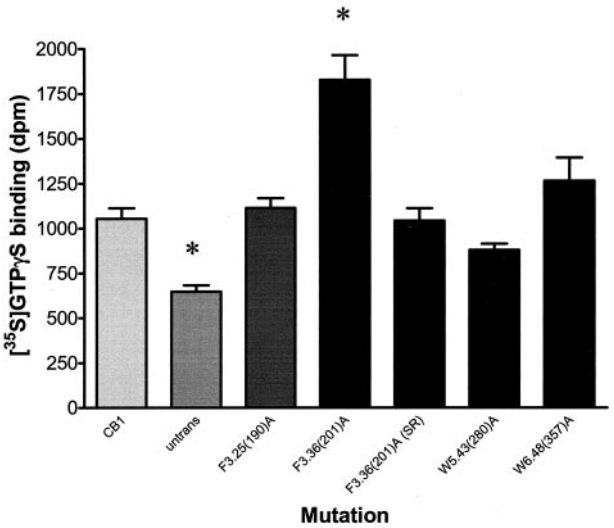

FIG. 7. **Agonist-independent activation of WT CB_1 and mutant receptors was assessed by measuring basal turnover of [^{35}S]GTPγS binding.** *(SR)* indicates reduction of basal [^{35}S]GTPγS binding in the presence of 1 μM SR141716A. Data shown are the mean ± S.E. of at least three experiments performed in triplicate. The * indicates statistically significant differences from wild type ($p < 0.05$).

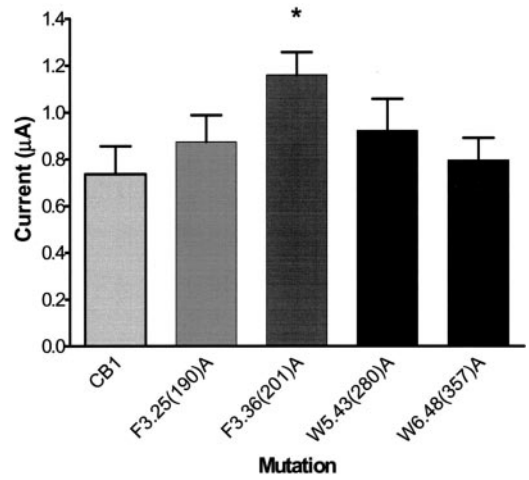

FIG. 8. **Agonist-independent activity of GIRK1/4 channels was assessed by measuring I_{HK} in oocytes expressing WT or mutant CB_1 receptors.** A large number of oocytes ($n = 20–46$) were analyzed for each condition from at least two batches of oocytes. The amount of RNA injected and the recording protocol are described under the "Experimental Procedures." The * indicates statistically significant differences from wild type (*, $p < 0.05$, one-way analysis of variance).

hydrogen bonds for the carbonyls at positions ($i - 3$) and ($i - 4$). Both the departure from the ideal helical pattern and the reduction in H-bond stabilization contribute to the observed flexibility of a proline-containing α-helix. Table V lists the results of ProKink analyses of WT TMH6 CM output and the W6.48A TMH6 CM output. This analysis yields values not only

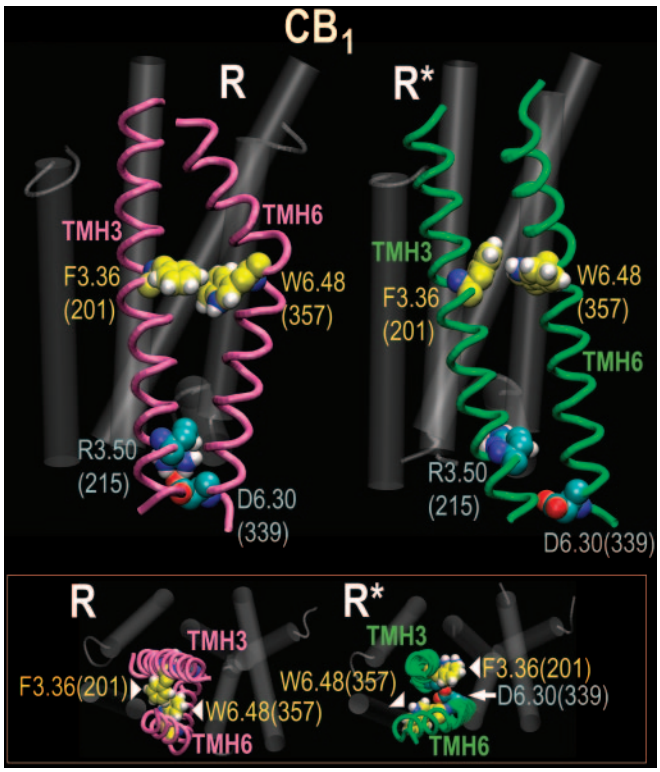

FIG. 9. **The relationship between F3.36(201) and W6.48(357) in the inactive (R) and active (R*) states of CB_1 as predicted by molecular modeling is illustrated here.** The major view is from TMH5 looking toward TMHs3/6. *Left,* in the R state, W6.48(357) adopts a g+ χ_1, whereas F3.36(201) adopts a trans χ_1. In this arrangement, W6.48(357) and F3.36(201) are engaged in an aromatic stacking interaction that stabilizes the R state. By analogy with Rho, the CB_1-inactive state is also characterized by a salt bridge between R3.50(215) and D6.30(339) at the intracellular side of CB_1 that keeps the intracellular ends of TMH3 and 6 close (3). The TMH6 kink extracellular to W6.48(357) permits a hypothesized salt bridge between K3.28(193) and D6.58 (367) to form (51). This salt bridge is made possible by the profound flexibility in TMH6 due to the presence of G6.49(358) in the CW*X*P motif of TMH6 (25). *Right,* in the R* state, W6.48(357) and F3.36(201) have moved apart due to rotation of TMH3 and -6 during activation. W6.48(357) has adopted a trans χ_1 and has moved toward the viewer and F3.36(201) has adopted a g+ χ_1 and has moved away from the viewer. The R3.50(215)/D6.30(339) salt bridge is broken, and the proline kink in TMH6 has moderated. *Inset,* this inset provides an extracellular view of CB_1. Here it is clear that in R, F3.36(201) and W6.48(357) are engaged in an aromatic stacking interaction, but in R*, F3.36(201) and W6.48(357) are no longer close enough to interact.

for the bend angle of this proline-containing helix but also the wobble angles and face shifts for these helices. The bend angle is the angle between the two parts when the helix is kinked along its axis. The wobble angle is the angle that defines the orientation of the post-proline helix in three-dimensional space, with respect to the pre-proline helix. The face shift measures the distortion that causes a twisting of the helix "face" in such a way that amino acids that used to be on the same side (face) of the helix are shifted and are on different sides of the helix as a result of the bend (20).

The results of conformational memories calculations on WT CB_1 and the W6.48A mutant are summarized in Table V. In each case, *X*-cluster identified two major clusters of conformers. The first cluster contained TMH6s with large bend angles, whereas the second cluster contained TMH6s with straighter helices (*i.e.* smaller bend angles). Because TMH6 is more kinked in the inactive state (R) and straightens in the activated state (R*), these two clusters are labeled R and R* in Table V (12). The ProKink program (20) was used to analyze each helix within each cluster in terms of bend angle, wobble angle, and face shift and to compute averages and standard deviations for each cluster.

For WT CB_1, cluster 1 contained 40 members with an average proline bend (kink) angle of 75.9 ± 1.0°, whereas cluster 2 contained 51 members with average bend angle of 33.7 ± 1.1°. The TMH6 used in our CB_1 R model was selected from the more bent cluster, cluster 1, whereas the TMH6 used in our CB_1 R* model was selected from the straighter cluster, Cluster 2 (see "Experimental Procedures"). For the TMH6 W6.48A mutant, cluster 1 contained 19 members with an average proline bend (kink) angle of 74.0 ± 1.0°, whereas cluster 2 contained 72 members with an average proline bend angle of 36.8 ± 1.2°.

At the 0.01 level, the difference of population means for the kink, wobble, and face shift angles for the W6.48A mutant reported in Table V were not significantly different from the corresponding measures in WT CB_1, except for the R* wobble angle. Here the W6.48A R* wobble angle (−105.6 ± 3.4°) was found to be significantly different from the WT R* wobble angle (−120.5 ± 4.6°) at the 0.01 level. Fig. 10 illustrates the steric consequence of this 15° difference in wobble angle. In the R to R* transition, the salt bridge between R3.50 and D/E6.30 is thought to be broken via a conformational change in TMH6 mediated by the flexible hinge region (CW*X*P motif) of TMH6. Fig. 10 shows that D6.30 in the W6.48A mutant is capable of pulling further away from the intracellular end of TMH3 and R3.50 than is D6.30 in WT TMH6.

DISCUSSION

Mutation of the toggle switch residues, F3.36(201) and W6.48(357), yielded perhaps the most interesting results of all aromatic microdomain mutations reported here. Mutation of F3.36(201) resulted in elevated basal signaling (increased constitutive activity) and reduced ligand efficacies. Mutation of W6.48(357) resulted in unaltered basal signaling but greatly enhanced ligand efficacies. These results are discussed below.

F3.36(201)A Mutation—F3.36(201) is revealed here to be a key residue both for ligand binding and for CB_1 activation. One of the significant results in the work reported here is that although WT CB_1 and the F3.36(201)A mutant have statistically equivalent protein expression levels in HEK293 cells (see Table I), an F3.36(201)A mutation results in a statistically significant higher level of ligand-independent activation of CB_1 (*i.e.* higher basal levels, increased constitutive activity) as assessed by [^{35}S]GTPγS binding. In addition to the demonstration of elevated basal levels, another way to test for constitutive activity in a mutant receptor is to examine the effects on basal signaling produced by an inverse agonist. If the receptor is constitutively active, then the inverse agonist should be able to reduce basal levels (*i.e.* reduce [^{35}S]GTPγS binding). We have shown here by assessing basal turnover of [^{35}S]GTPγS binding, that the CB_1 inverse agonist, SR141716A reduces basal signaling in the F3.36(201)A mutant, and this effect is statistically significant ($p < 0.05$) (see Fig. 7 and Table IV). Another traditional expectation of constitutively active receptors is that the affinities of agonists should increase, and the affinities of inverse agonists should decrease due to the shift in the receptor population toward R*. The majority of GPCR mutations that have led to constitutive activity has been mutations in the intracellular half-of the TMH bundle, away from the ligand-binding pocket. Very typically, these have been mutations to TMH6 (45). However, the mutation that produced an increase in constitutive activity here, F3.36(201)A, involves a key residue in the ligand-binding pocket. For this reason, measured ligand affinities for agonists, for example, would be the result of two opposing factors as follows: an increase in affinity due to the higher percentage R* in the F3.36(201)A mutant, but a

TABLE V
Results of conformational memories study of WT versus W6.48(357)A TMH6

	No. members	Bend angle	Wobble angle	Face shift
		degrees ± S.E.	*degrees ± S.E.*	*degrees ± S.E.*
WT				
R CLS 1	40	75.9 ± 1.0	−47.5 ± 8.2	60.3 ± 4.1
R* CLS 2	51	33.7 ± 1.1	−120.5 ± 4.6	57.8 ± 7.0
W6.48(357)A				
R CLS 1	19	74.0 ± 1.0	−39.6 ± 1.8	60.9 ± 2.2
R* CLS 2	72	36.8 ± 1.2	−105.6[b] ± 3.4	59.6 ± 5.9

[a] CLS, cluster.
[b] Statistically significant difference from WT at the $p = 0.01$ level.

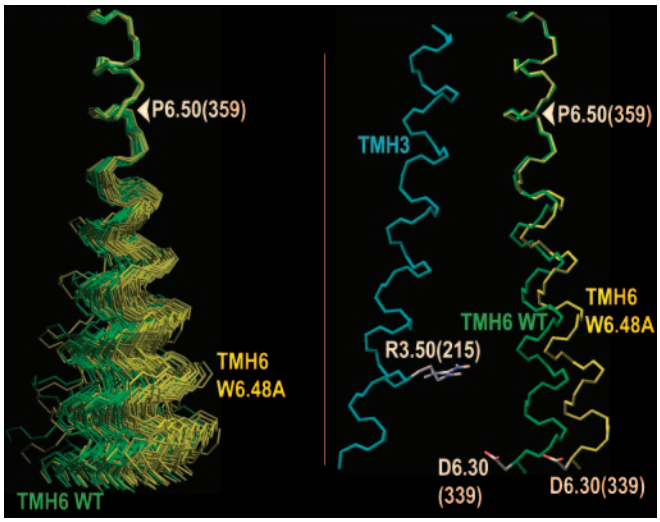

FIG. 10. **A comparison of conformational memories results for WT CB_1 TMH6 and the CB_1 W6.48A TMH6 mutant.** *Left,* here the WT CB_1 TMH6 R* cluster in *green* (51 members, see Table V) is shown superimposed at their extracellular ends with the CB_1 W6.48A TMH6 mutant R* cluster in *yellow* (72 members, see Table V). Statistically, these two clusters differed only in their wobble angles (see Table V). The view is through the plane of the proline kink. Here it is clear that the wobble angle difference between the two groups results in a change in the three-dimensional placement of the intracellular ends of these two clusters. *Right,* a single helix from the WT R* cluster (bend angle = 33.8° and wobble angle = −120.9°) and a single helix from the W6.48A R* cluster (bend angle = 35.5° and wobble angle = −105.1°) are shown here superimposed at their extracellular ends and positioned inside the R* bundle. These helices have similar bend angles but differ by 15.8° in their wobbles angles. The receptor state symbolized in the figure is the activated (R*) state. The counterclockwise (from extracellular perspective) rotations of TMH3 and -6 and the straightening of TMH6 upon activation result in the loss of the R3.50(215)/D6.30(339) salt bridge as R3.50(215) and D6.30(339) move away from each other, opening a space between TMH3 and -6 at their intracellular ends. It is clear here that the change in wobble angle between the WT TMH6 (*green*) and W6.48A mutant TMH6 (*yellow*) results in a greater displacement of D6.30(339) relative to R3.50(215) in the W6.48A mutant (*yellow*).

decrease in affinity (some likely more than others depending on binding site) due to a change in the ligand-binding site interactions and/or in the binding pocket itself. For this reason, it is not appropriate to use a shift in ligand affinities as a test for constitutive activity here.

The W6.48(357)/F3.36(201) Toggle Switch in WT CB_1—In recently published Monte Carlo/stochastic dynamics calculations on the inactive state of CB_1, we found that one of the most persistent aromatic stacking interactions in the inactive state of CB_1 is the F3.36(201)/W6.48(357) interaction (46). Models of the CB_1 inactive (R) and active (R*) TMH bundles illustrated here in Fig. 9 show that in the inactive state residues W6.48(357)(χ_1 = g+) and F3.36(201) (χ_1 = trans) are engaged in a direct aromatic stacking interaction. In this interaction, F3.36(201) appears to serve the function of confining W6.48(357) to the g+ χ_1 rotamer state and restricting movement of W6.48. In Rho, the β-ionone ring of 11-*cis*-retinal appears to serve the same function as F3.36(201) in CB_1 (3, 14) (Fig. 11), *i.e.* it sterically confines W6.48(265) to the g+ χ_1 rotamer state and restricts the movement of W6.48. Khorana and co-workers (13) have recently reported one of the specific contacts that must break in Rho for activation involves W6.48(265).

The conformational changes that occur upon receptor activation result in rotations of TMH3 and -6, as well as a change in the conformation of TMH6 (by moderation of its proline kink angle) (6–8,12). In the light-activated state of Rho, the β-ionone ring moves away from TMH F and toward TMH D where it resides close to A4.58(169) (14). This movement releases the constraint on W6.48, making it possible for W6.48(265) to undergo a conformational change. For the CB_1 receptor, counterclockwise (from the extracellular side) rotations of TMH3 and -6 concomitant with activation (26, 32) would move F3.36(201) and W6.48(357) past each other, with W6.48(357) moving toward the viewer in Fig. 11 and F3.36(201) moving away from the viewer (also see Fig. 9). Our modeling studies of the CB_1 TMH bundle suggest that these rotations cannot take place without a rotamer change for both W6.48(357) and F3.36(201) due to steric clashing. In our models, activation is accompanied by a χ_1 change in W6.48(357) from g+ → trans and a χ_1 change in F3.36(201) from trans → g+ (see above and Fig. 9). The W6.48(357)/F3.36(201) interaction may act as the toggle switch for CB_1 activation, with W6.48(357) χ_1 g+/F3.36(201) χ_1 trans representing the inactive and W6.48(357) χ_1 trans/F3.36(201) χ_1 g+ representing the active state of CB_1 (see Fig. 9). If this is true, then mutation of F3.36(201) to a smaller residue, a residue that is no longer a steric block to conformational change in W6.48, would be expected to increase ligand-independent activation of CB_1, and this is what is seen here experimentally.

Whereas the F3.36(201)A mutation leads to a high degree of constitutive activity as is indicated in Fig. 7, this mutation also results in the reduced efficacy for WIN and CP. This reduction cannot be explained simply by reduced ligand affinity, as the affinity of CP is not affected by this mutation, but its efficacy is affected. It is possible that because the WT CB_1 receptor itself exhibits a high level of constitutive activity (33–35) and because the F3.36(201)A mutant exhibits an increase in constitutive activity relative to WT CB_1, the population of F3.36(201)A mutant receptors is already shifted heavily toward R*. This should not interfere with agonist binding, as agonists have higher affinity for the R* state. However, this would leave fewer receptors for ligands to activate, resulting in a reduced E_{max}. This explanation is consistent with that of Milligan (45) in a recent review concerning constitutive activity of GPCRs. Milligan (45) noted that "a number of GPCRs do seem to have significant levels of constitutive activity when expressed in cell lines; in some cases, ligand-induced stimulation of activity is relatively small compared with the signal in the absence of ligand" (45). Alternatively, the profound effect on ligand-dependent activation seen here for the F3.36(201)A mutation may indicate that aromaticity at residue 3.36 is cen-

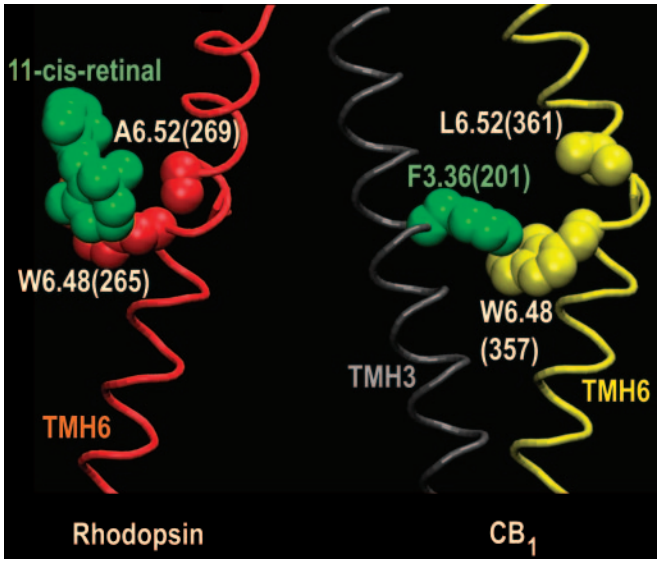

FIG. 11. **Inactive state (R) three-dimensional representations of the similar orientations of 11-*cis*-retinal/W6.48(265) in Rho (3) and the F3.36(201)/W6.48(357) pair in CB_1.** The view is from TMH5 looking toward TMH6. Activation will cause TMH6 to undergo a counterclockwise rotation (from extracellular view) (26). This will cause W6.48(357) to rotate toward the viewer. *Left*, the β-ionone ring of 11-*cis*-retinal constrains W6.48(265) in a g+ χ_1 in the dark (inactive) state of rhodopsin and opposes rotation of TMH6 (3). *Right*, F3.36(201) in a trans χ_1 constrains W6.48(357) in a g+ χ_1 in the CB_1 inactive state model and opposes rotation of TMH6.

tral to the CB_1 agonist-induced activation process and, consequently, that mutation to a nonaromatic residue impairs the function of this mutant CB_1.

W6.48(357)A Mutation—The W6.48(357)A mutation did not result in a statistically significant change in basal levels relative to WT CB_1 (see Fig. 7). Our CB_1 modeling studies have shown that when W6.48(357) is mutated to alanine, helix packing allows F3.36(201) to interact with both A6.48 and L6.51. This interaction would serve the same function as F3.36(201) serves in WT CB_1, *i.e.* effectively helping to stabilize TMH6 in its inactive state conformation. Therefore, these results suggest that basal levels should not change between WT CB_1 and the W6.48(357)A mutant. Looking at this from another perspective, consideration of the changes in the aromatic microdomain as a result of this mutation also suggests that aromatic stacking in both the R and R* states will be equally impacted by the W6.48(357)A mutation (see "Results"), it is reasonable then to expect that the W6.48(357)A mutant will not produce a change in basal levels relative to WT CB_1, and this is what was seen experimentally.

Although the W6.48(357)A mutation had no effect on basal levels, it had noticeable effects on ligand-induced activation, such that the efficacy of every ligand tested was enhanced. One of the steps that has been proposed to occur during GPCR activation is the breaking of an ionic lock (salt bridge) between R3.50 and E/D6.30 that constrains the intracellular ends of TMH3 and TMH6 to remain close in the inactive state (see Fig. 9, *left*) (10). GPCR activation appears to open a cleft at the cytoplasmic face of a GPCR. Meng and Bourne (47) have described activation as a "blossoming open" of the receptor at its intracellular end. This opening permits G protein docking and interaction with the cytoplasmic domains of the receptor. In Rho, upon light activation, receptor residues in the IC-2 and IC-3 loops have been cross-linked with the C terminus of the Gα protein subunit and residues in the a4-b6 loop of Gα, indicating that these sites on the Gα subunit are receptor-binding sites (48). It is clear from the conformational memories results reported here in Table V that the accessible conformations of TMH6 are altered by the W6.48A mutation, with a 15° change in the wobble angle for the population of W6.48(357)A TMH6 R*, compared with that of the R* WT CB_1 TMH6 population. As illustrated in Fig. 10, this change leads to TMH6 conformations in which D6.30(339) in TMH6 is pulled further back from R3.50(215) in TMH3, resulting in a wider "blossomed" intracellular end of CB_1 in the TMH6 W6.48(357)A mutant. Such a wider opening may permit better coupling between the G protein and the W6.48(357)A mutant upon ligand activation, thus resulting in increased E_{max} values.

This phenomenon of dramatic enhancement of E_{max} values upon mutation of residue W6.48(357) has been seen previously in the CCK-B gastrin receptor (49). Blaker and co-workers (49) found that whereas a W6.48(346)A mutation did not affect basal inositol phosphate production, this mutation affected the functional activity of PD-135,158 (from 20 ± 1% for WT CCK-B to 43 ± 5% in the W6.48(346)A mutant). An enhancement of E_{max} has also been seen previously for mutations at other loci. For example, in the δ-opioid receptor, Befort and co-workers (50) found that a Y308F mutation in TMH7 resulted in a marked increase in the efficacy of the potent agonist BW373U86. Consistent with the interpretation of the CB_1 W6.48(357)A mutation discussed above, these authors (50) attributed this increase to a change in the receptor active state conformation, such that the receptor can interact with heterotrimeric G proteins more effectively.

Conclusions—Modeling, mutation, and functional studies undertaken to test the importance of the TMH3-4-5-6 aromatic microdomain in ligand recognition and in the conformational changes that accompany activation of CB_1 suggest that a F3.36(201)/W6.48(357)-specific contact is an important constraint for the CB_1-inactive state that may need to break during activation. Modeling studies suggest that the F3.36(201)/W6.48(357) contact can exist in the inactive state of CB_1 and be broken in the activated state via a χ_1 rotamer switch (F3.36(201) trans, W6.48(357) g+) → (F3.36(201) g+, W6.48(357) trans). The F3.36(201)/W6.48(357) interaction, therefore, may represent a toggle switch for activation of CB_1.

REFERENCES

1. McAllister, S. D., Rizvi, G., Anavi-Goffer, S., Hurst, D. P., Barnett-Norris, J., Lynch, D. L., Reggio, P. H., and Abood, M. E. (2003) *J. Med. Chem.* **46,** 5139–5152
2. Gerard, C. M., Mollereau, C., Vassart, G., and Parmentier, M. (1991) *Biochem. J.* **279,** 129–134
3. Palczewski, K., Kumasaka, T., Hori, T., Behnke, C. A., Motoshima, H., Fox, B. A., Le Trong, I., Teller, D. C., Okada, T., Stenkamp, R. E., Yamamoto, M., and Miyano, M. (2000) *Science* **289,** 739–745
4. Okada, T., Fujiyoshi, Y., Silow, M., Navarro, J., Landau, E. M., and Shichida, Y. (2002) *Proc. Natl. Acad. Sci. U. S. A.* **99,** 5982–5987
5. Reggio, P. H., Basu-Dutt, S., Barnett-Norris, J., Castro, M. T., Hurst, D. P., Seltzman, H. H., Roche, M. J., Gilliam, A. F., Thomas, B. F., Stevenson, L. A., Pertwee, R. G., and Abood, M. E. (1998) *J. Med. Chem.* **41,** 5177–5187
6. Farrens, D., Altenbach, C., Ynag, K., Hubbell, W., and Khorana, H. (1996) *Science* **274,** 768–770
7. Gether, U., Lin, S., Ghanouni, P., Ballesteros, J., Weinstein, H., and Kobilka, B. (1997) *EMBO J.* **16,** 6737–6747
8. Ghanouni, P., Steenhuis, J. J., Farrens, D. L., and Kobilka, B. K. (2001) *Proc. Natl. Acad. Sci. U. S. A.* **98,** 5997–6002
9. Ballesteros, J. A., Shi, L., and Javitch, J. A. (2001) *Mol. Pharmacol.* **60,** 1–19
10. Ballesteros, J., Jensen, A., Liapakis, G., Rasmussen, S., Shi, L., Gether, U., and Javitch, J. (2001) *J. Biol. Chem.* **276,** 29171–29177
11. Visiers, I., Ebersole, B. J., Dracheva, S., Ballesteros, J., Sealfon, S. C., and Weinstein, H. (2002) *Int. J. Quantum Chem.* **88,** 65–75
12. Jensen, A. D., Guarnieri, F., Rasmussen, S. G., Asmar, F., Ballesteros, J. A., and Gether, U. (2001) *J. Biol. Chem.* **276,** 9279–9290
13. Klein-Seetharaman, J., Yanamala, N. V., Javeed, F., Reeves, P. J., Getmanova, E. V., Loewen, M. C., Schwalbe, H., and Khorana, H. G. (2004) *Proc. Natl. Acad. Sci. U. S. A.* **101,** 3409–3413
14. Borhan, B., Souto, M. L., Imai, H., Shichida, Y., and Nakanishi, K. (2000) *Science* **288,** 2209–2212
15. Lin, S., and Sakmar, T. (1996) *Biochemistry* **35,** 11149–11159
16. Shi, L., Liapakis, G., Xu, R., Guarnieri, F., Ballesteros, J. A., and Javitch, J. A. (2002) *J. Biol. Chem.* **277,** 40989–40996
17. Ballesteros, J. A., and Weinstein, H. (1995) *Methods Neurosci.* **25,** 366–428
18. Guarnieri, F., and Weinstein, H. (1996) *J. Am. Chem. Soc.* **118,** 5580–5589

19. Mohamadi, F., Richards, N. G. J., Guida, W. C., Lizkamp, R., Lipton, M., Caulfield, C., Chang, G., Hendickson, T., and Still, W. C. (1990) *J. Comp. Chem.* **11,** 440–467
20. Visiers, I., Braunheim, B. B., and Weinstein, H. (2000) *Protein Eng.* **13,** 603–606
21. Deleted in proof
22. Abood, M. E. (1997) *Biochem. Pharmacol.* **53,** 207–214
23. Bramblett, R. D., Panu, A. M., Ballesteros, J. A., and Reggio, P. H. (1995) *Life Sci.* **56,** 1971–1982
24. Barnett-Norris, J., Hurst, D. P., Lynch, D. L., Guarnieri, F., Makriyannis, A., and Reggio, P. H. (2002) *J. Med. Chem.* **45,** 3649–3659
25. Barnett-Norris, J., Hurst, D. P., Buehner, K., Ballesteros, J. A., Guarnieri, F., and Reggio, P. H. (2002) *Int. J. Quantum Chem.* **88,** 76–86
26. Javitch, J. A., Fu, D., Liapakis, G., and Chen, J. (1997) *J. Biol. Chem.* **272,** 18546–18549
27. Burley, S. K., and Petsko, G. A. (1985) *Science* **229,** 23–28
28. Hunter, C. A., Singh, J., and Thornton, J. M. (1991) *J. Mol. Biol.* **218,** 837–846
29. Gallivan, J. P., and Dougherty, D. A. (1999) *Proc. Natl. Acad. Sci. U. S. A.* **96,** 9459–9464
30. Tao, Q., McAllister, S. D., Andreassi, J., Nowell, K. W., Cabral, G. A., Hurst, D. P., Bachtel, K., Ekman, M. C., Reggio, P. H., and Abood, M. E. (1999) *Mol. Pharmacol.* **55,** 605–613
31. McAllister, S., Griffin, G., Satin, L., and Abood, M. (1999) *J. Pharmacol. Exp. Ther.* **291,** 618–626
32. Hulme, E. C., Lu, Z. L., Ward, S. D., Allman, K., and Curtis, C. A. (1999) *Eur. J. Pharmacol.* **375,** 247–260
33. Bouaboula, M., Perrachon, S., Milligan, L., Canat, X., Rinaldi-Carmona, M., Portier, M., Barth, F., Calandra, B., Pecceu, F., Lupker, J., Maffrand, J.-P., LeFur, G., and Casellas, P. (1997) *J. Biol. Chem.* **272,** 22330–22339
34. Pan, X., Ikeda, S., and Lewis, D. (1998) *Mol. Pharmacol.* **54,** 1064–1072
35. Meschler, J. P., Kraichely, D. M., Wilken, G. H., and Howlett, A. C. (2000) *Biochem. Pharmacol.* **60,** 1315–1323
36. Mato, S., Pazos, A., and Valdizan, E. M. (2002) *Eur. J. Pharmacol.* **443,** 43–46
37. Kearn, C., Greenberg, M., DiCamelli, R., Kurzawa, K., and Hillard, C. (1999) *J. Neurochem.* **72,** 2379–2387
38. Chan, K. W., Langan, M. N., Sui, J. L., Kozak, J. A., Pabon, A., Ladias, J. A., and Logothetis, D. E. (1996) *J. Gen. Physiol.* **107,** 381–397
39. MacLennan, S., Reynen, P., Kwan, J., and Bonhaus, D. (1998) *Br. J. Pharmacol.* **124,** 619–622
40. Kenakin, T. (1997) *Pharmacologic Analysis of Drug-Receptor Interaction*, 3rd Ed., Lippincott-Raven, Philadelphia
41. Griffin, G. R., Atkinson, P. J., Showalter, V. M., Martin, B. R., and Abood, M. E. (1998) *J. Pharmacol. Exp. Ther.* **285,** 553–560
42. Hobohm, U., Scharf, M., Schneider, R., and Sander, C. (1992) *Protein Sci.* **1,** 409–417
43. Hobohm, U., and Sander, C. (1994) *Protein Sci.* **3,** 522–524
44. Sansom, M. S., and Weinstein, H. (2000) *Trends Pharmacol. Sci.* **21,** 445–451
45. Milligan, G. (2003) *Mol. Pharmacol.* **64,** 1271–1276
46. McAllister, S. D., Tao, Q., Barnett-Norris, J., Buehner, K., Hurst, D. P., Guarnieri, F., Reggio, P. H., Nowell Harmon, K. W., Cabral, G. A., and Abood, M. E. (2002) *Biochem. Pharmacol.* **63,** 2121–2136
47. Meng, E. C., and Bourne, H. R. (2001) *Trends Pharmacol. Sci.* **22,** 587–593
48. Hamm, H. E. (2001) *Proc. Natl. Acad. Sci. U. S. A.* **98,** 4819–4821
49. Blaker, M., Ren, Y., Seshadri, L., McBride, E. W., Beinborn, M., and Kopin, A. S. (2000) *Mol. Pharmacol.* **58,** 399–406
50. Befort, K., Zilliox, C., Filliol, D., Yue, S., and Kieffer, B. L. (1999) *J. Biol. Chem.* **274,** 18574–18581
51. Hurst, D. P., Lynch, D. L., Barnett-Norris, J., Hyatt, S. M., Seltzman, H. H., Zhong, M., Song, Z. H., Nie, J., Lewis, D., and Reggio, P. H. (2002) *Mol. Pharmacol.* **62,** 1274–1287

Structural Mimicry in Class A G Protein-coupled Receptor Rotamer Toggle Switches: THE IMPORTANCE OF THE F3.36(201)/W6.48(357) INTERACTION IN CANNABINOID CB1 RECEPTOR ACTIVATION

Sean D. McAllister, Dow P. Hurst, Judy Barnett-Norris, Diane Lynch, Patricia H. Reggio and Mary E. Abood

J. Biol. Chem. 2004, 279:48024-48037.
doi: 10.1074/jbc.M406648200 originally published online August 23, 2004
